

Comparison of Ballistic Transport Characteristics of Monolayer Transition Metal Dichalcogenides (TMDs) MX_2 ($\text{M} = \text{Mo}, \text{W}; \text{X} = \text{S}, \text{Se}, \text{Te}$) n-MOSFETs

Jiwon Chang, Leonard F. Register and Sanjay K. Banerjee
 Microelectronics Research Center,
 The University of Texas at Austin,
 10100 Burnet Road, Bldg. 160, Austin, TX 78758, U.S.A
 jiwon.chang@utexas.edu

Abstract—We study the transport properties of monolayer transition metal dichalcogenides (TMDs) MX_2 ($\text{M} = \text{Mo}, \text{W}; \text{X} = \text{S}, \text{Se}, \text{Te}$) n-channel metal-oxide-semiconductor field effect transistors (MOSFETs) using an atomistic tight-binding full-band ballistic quantum transport simulations, with hopping potentials obtained from density functional theory. We discuss the subthreshold slope (SS), drain-induced barrier lowering (DIBL), as well as gate-induced drain leakage (GIDL) for different monolayer MX_2 MOSFETs. We also report the possibility of negative differential resistance to the extent quasi-ballistic transport exists in such nanostructure TMD MOSFETs.

Keywords—component; transition metal dichalcogenides, atomistic, quantum transport

I. INTRODUCTION

In past few years, transition metal dichalcogenides (TMDs) have been intensively explored for the next generation devices. TMDs with a chemical formula MX_2 , where M is a transition metal atom and X is one of the chalcogens such as S, Se and Te, are composed of stacks of multiple X-M-X layers. One X-M-X layer (monolayer MX_2) consists of an M atom layer sandwiched between two X atom layers. The M-X bonding is strongly covalent, but the X-M-X layers are coupled only by weak van der Waals forces. Therefore, micromechanical

exfoliation can be used to fabricate and isolate atomically thin MX_2 layers [1,2]. Due to the nearly two-dimensional (2-D) nature, monolayer TMDs can provide a higher degree of electrostatic control than conventional bulk materials, making them promising for low power switching.

Strong dependency of band structures on the number of X-M-X layers has been found by both theoretical [3,4,5] and experimental [1] studies on various MX_2 ($\text{M} = \text{Mo}, \text{W}; \text{X} = \text{S}, \text{Se}, \text{Te}$). Multilayer MX_2 has an indirect band gap while a direct band gap is observed in the monolayer MX_2 . An n-channel metal-oxide-semiconductor field effect transistor (n-MOSFETs) with the monolayer MoS_2 was reported with high mobility, high ON-OFF current ratio and ultralow standby power dissipation [6]. A high performance p-channel MOSFETs (p-MOSFETs) using monolayer WSe_2 was also demonstrated experimentally [7]. Theoretical studies based on the ballistic transport within an effective mass approximation, have estimated the performance limits of monolayer MX_2 MOSFETs [8,9]. In this work, we consider full band effects on the limits of ballistic transport in TMD n-MOSFETs via atomistic tight-binding quantum transport simulations, with hopping potentials obtained from density functional theory.

II. COMPUTATIONAL APPROACH

The primitive unit cell of monolayer TMDs MX_2 is hexagonal with lattice parameters a and c (Fig. 1(a) and 1(b)). We construct the lattice structure of monolayer MX_2 by using experimental lattice parameters listed in Table I [10]. We use OPENMX [11] to perform DFT calculations within the local density approximation (LDA) [12]. For all considered monolayer MX_2 systems, a direct band gap at K in the hexagonal Brillouin zone is obtained from DFT calculations. For reference only, the estimated electron effective masses near the conduction band (CB) minimum in the direction Γ -K in Table I tend to increase for heavier X atoms with the same M atom. With the same X atom, electron effective masses of WX_2 are lighter than those of MoX_2 . The simulated device structure of monolayer MX_2 MOSFETs is illustrated in Fig. 1(c). We consider 15 nm channel length n-MOSFETs. The undoped monolayer MX_2 is on top of a 50 nm thick SiO_2 substrate is

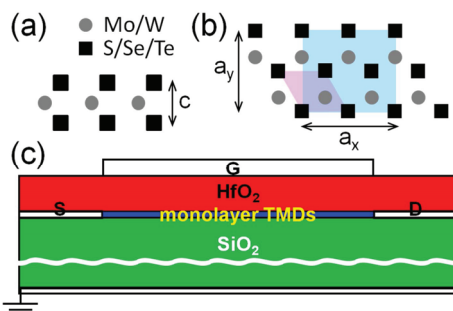


Figure 1. (a) Side and (b) top views of monolayer TMDs. Hexagonal (magenta) and rectangular (green) unit cells are shown. (c) Device structure of monolayer TMD MOSFETs. The nominal device parameters are as follows: HfO_2 ($\kappa = 25$) gate oxide thickness = 2.8 nm, channel length = 15 nm, n-type doping density of source and drain = $7 \times 10^{13} \text{ cm}^{-2}$ and SiO_2 oxide thickness = 50 nm.

This work was supported by the Nanoelectronics Research Initiative's Southwest Academy of Nanoelectronics (NRI-SWAN) center, and Intel. Supercomputing resources were provided by the Texas Advanced Computing Center (TACC).

TABLE I. LATTICE CONSTANTS, DIRECT BAND GAP SIZES, ELECTRON EFFECTIVE MASSES AND DIELECTRIC CONSTANTS OF MONOLAYER MX_2 .

MX_2	Lattice Constant		Band Gap [eV]	m_e^*/m_e	Dielectric Constant
	a_x	c [Å]			
MoS₂	3.160	3.172	1.8	0.56	4.8
MoSe₂	3.299	3.352	1.51	0.62	6.9
MoTe₂	3.522	3.630	1.10	0.64	8.0
WS₂	3.155	3.160	1.93	0.33	4.4
WSe₂	3.286	3.376	1.62	0.35	4.5

gated through 2.8 nm thick HfO_2 gate insulator. The source and drain are n-type doped to a carrier concentration of $7 \times 10^{13} \text{ cm}^{-2}$. The relative dielectric constant of each monolayer MX_2 used in the work is listed in Table 1 [13]. The TB Hamiltonian including non-nearest neighbor inter-atom coupling is obtained from DFT using maximally localized Wannier functions (MLWFs) [14]. We inject the eigenmodes of the semi-infinite source and drain, and use recursive scattering matrices to propagate injected carrier wavefunctions through the device from the source (drain) to the drain (source) [15]. For this latter purpose, the monolayer MX_2 is divided into a series of rectangular unit cells marked with a green rectangular in Fig. 1(b). In this way, despite the non-nearest neighbor inter-atom coupling, there only nearest neighbor coupling among unit cells compatible with the method of [15]. Current is calculated by integrating transmission coefficients over energy with a Fermi function weight. Transport calculations are performed together with a Poisson solver until self-consistency between the charge density and electrostatic potential is obtained.

III. RESULTS AND DISCUSSION

Simulation results of monolayer MX_2 n-MOSFETs are presented in Figs. 2 and 3. For all MX_2 monolayers considered here, good subthreshold behaviors and small short-channel effects are observed from the transfer characteristics, I_{DS} vs. $V_{\text{GS}} - V_{\text{T}}$, in Fig. 2. The subthreshold slope (SS) and drain-induced barrier lowering (DIBL) estimated for each monolayer MX_2 are provided in Table II. Among the monolayer MoX_2 (MoS_2 , MoSe_2 , MoTe_2) n-MOSFETs, MoS_2 shows the smallest SS ($\sim 60 \text{ mV/dec}$) and DIBL ($\sim 10 \text{ mV/V}$). With a heavier X (Se, Te) atom form MoSe_2 and MoTe_2 , both SS and DIBL increase, but remain relatively small. This slight degradation can be explained by the larger dielectric constant of MoSe_2 and MoTe_2 as compared to that of MoS_2 . With a higher dielectric constant, the lateral electric field from drain becomes more influential on the channel, leading to the increase of SS and DIBL. However, with only a monolayer of TMD, the dielectric environment is still dominated by the substrate and gate material, mitigating the detrimental effects of increasing TMD dielectric constant. The SS and DIBL for two different monolayer WX_2 (WS_2 , WSe_2) n-MOSFETs are alike due to the similarity in the dielectric constant and the effective mass as seen in Table II. All WX_2 n-MOSFETs have somewhat better SS

TABLE II. SS AND DIBL FOR MONOLAYER MoS_2 n-MOSFETS.

MX_2	SS [mV/dec]	DIBL [mV/V]
MoS₂	~ 60	~ 10
MoSe₂	~ 65	~ 15
MoTe₂	~ 70	~ 20
WS₂	~ 60	~ 7
WSe₂	~ 63	~ 10

and DIBL as compared to MoSe_2 and MoTe_2 n-MOSFETs, mainly due to the smaller dielectric constant. The SS and DIBL of monolayer WS_2 , WSe_2 , and MoS_2 n-MOSFETs are found to be very close. For all monolayer MX_2 n-MOSFETs except the monolayer MoTe_2 device, gate-induced drain leakage (GIDL), a potentially significant component of OFF-state leakage current in materials such as Si and common III-Vs, is not possible within the voltage ranges considered here due to the large band gaps (which, if anything, would be underestimated via the LDA DFT calculations). For monolayer MoTe_2 , devices, however, the simulated subthreshold currents does show an increase for very low gate voltages, below $V_{\text{GS}} - V_{\text{T}} \approx -0.7 \text{ V}$. Because of its relatively smaller band gap ($\sim 1.1 \text{ eV}$), there exists an overlap between CB and VB in the region between the channel and drain with the low $V_{\text{GS}} - V_{\text{T}}$, which allows channel-to-drain band-to-band tunneling. This latter small current was calculated using the self-consistent potential profiles obtained without considering GIDL, and then injecting current into the valence band directly beneath the channel barrier top.

The linear scale plots of I_{DS} vs. $V_{\text{GS}} - V_{\text{T}}$ in Fig. 2 exhibit significantly better transconductance at $V_{\text{DS}} = 0.5 \text{ V}$ for the WX_2 TMDs as compared to the MoX_2 TMDs in these ballistic simulations. Moreover, the MoX_2 TMDs show limited improvement in transconductance from $V_{\text{DS}} = 0.05 \text{ V}$ to $V_{\text{DS}} = 0.5 \text{ V}$ unlike the WX_2 TMDs. The reason for this difference becomes clear from Fig. 3, where it is seen that the MoX_2 TMD devices exhibit substantial NDR, as previously discussed

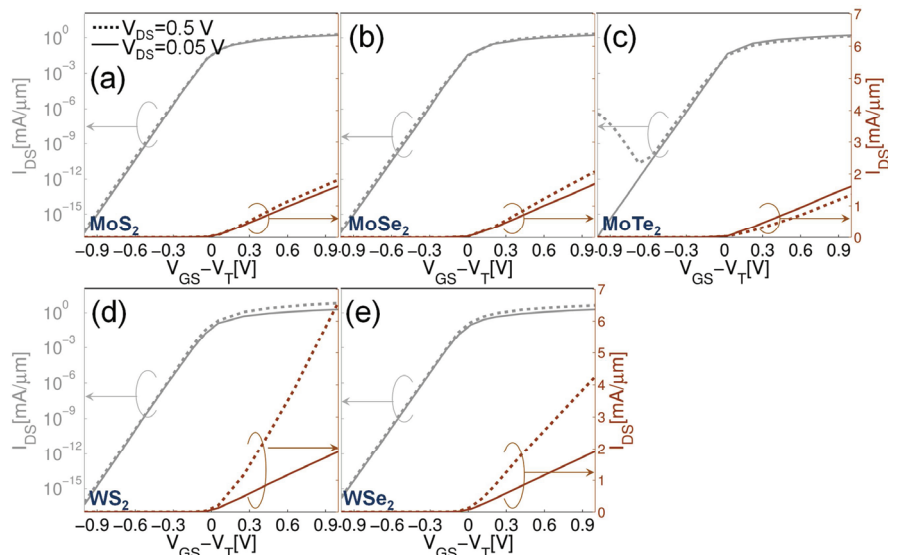


Figure 2. I_{DS} vs. $V_{\text{GS}} - V_{\text{T}}$ of 15 nm channel length monolayer (a) MoS_2 , (b) MoSe_2 , (c) MoTe_2 , (d) WS_2 , and (e) WSe_2 n-MOSFETs at $V_{\text{DS}} = 0.05$ and 0.5 V .

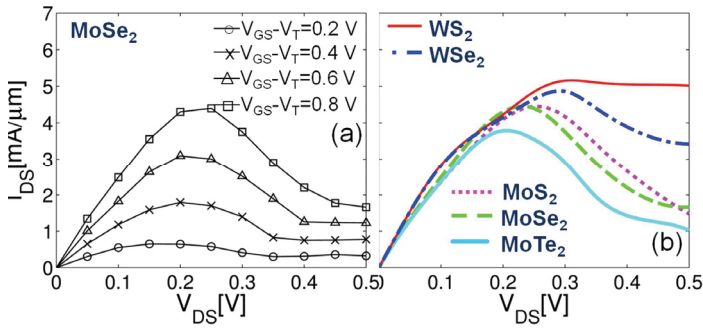


Figure 3. (a) I_{DS} vs. V_{DS} curves of 15 nm channel length monolayer MoSe₂ n-MOSFETs at $V_{GS}-V_T = 0.2, 0.4, 0.6,$ and 0.8 V. (b) Comparison of I_{DS} vs. V_{DS} curves of various 15 nm channel length monolayer MX₂ n-MOSFETs at $V_{GS}-V_T = 0.8$.

for MoS₂ [16] while the WX₂ TMD devices exhibit some but much less NDR. Indeed, up to about $V_{DS} = 0.2$ V, all devices show much the same transconductance.

To illustrate the source of NDR, we follow the transmission probabilities for transverse momentum $k_y = 0$ as a function of drain voltage V_{DS} in monolayer MoSe₂ n-MOSFETs. Fig. 4 contains six sub-figures corresponding to $V_{DS} = 0.0, 0.1, 0.2, 0.3, 0.4$ and 0.5 V, respectively. Each sub-figure has two CB plots at $k_y = 0$ on the left-hand-side (LHS), one in the source (black lines) and the other in the drain, except at $V_{DS} = 0.0$ V where two CBs plots overlap. The right-hand sides (RHSs) show transmission probabilities for $k_y = 0$ totaled over incident states/modes as a function of energy. Here only, to isolate the full band structure effects, we used a piecewise linear potential approximation for the source, channel and drain for the different drain biases. We consider transmission from the incident modes in the source lead to the outgoing modes in the drain lead. In the LHS of Fig 4(a) with $V_{DS} = 0$ V, two

TABLE III. TRANSMISSION PROBABILITIES BETWEEN INDIVIDUAL SOURCE AND DRAIN MODES OF FIXED SPIN FOR DIFFERENT DRAIN BIASES OF $V_{DS} = 0.1, 0.2, 0.3, 0.4,$ AND 0.5 V IN MONOLAYER MOSE2 N-MOSFETs.

V_{DS} [V]	Probabilities						
0.0							
	S	D	1	2			
	1	1.00000	0.00000				
	2	0.00000	1.00000				
0.1							
	S	D	1	2			
	1	0.99970	0.00000				
	2	0.00001	0.94617				
0.2							
	S	D	1	2	3	4	
		1	0.99901	0.00000	0.00001	0.00006	
		2	0.00003	0.96740	0.00273	0.00000	
0.3							
	S	D	1	2	3	4	5
		1	0.89504	0.00009	0.00264	0.01323	0.00526
		2	0.00004	0.96472	0.00178	0.00021	0.01254
	0.4						
S		D	1				
	1	0.97366					
	2	0.01817					
0.5							
	S	D	1				
	1	0.96542					
	2	0.02242					

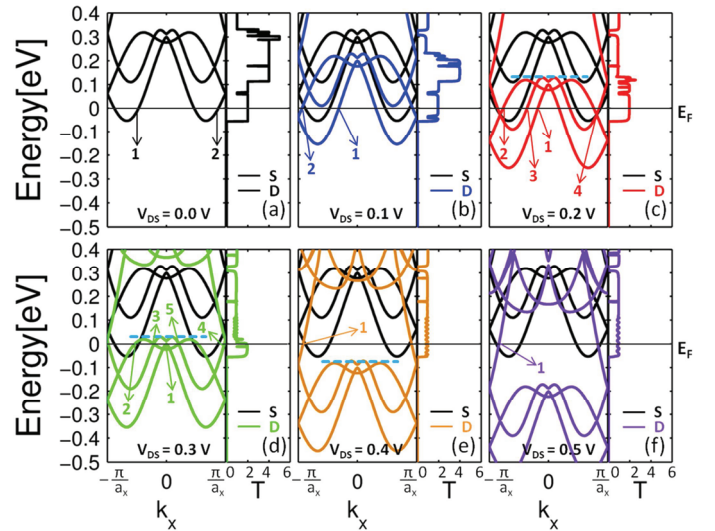


Figure 4. CB band structure of monolayer MoSe₂ for transverse mode $k_y = 0$, with the zero energy reference defined by an n-type doping density of $7 \times 10^{13} \text{ cm}^{-2}$. The indicated energy levels correspond to NDR behavior as described in the text.

incoming modes not counting spin degeneracy here, as well as their equivalent outgoing modes are labeled by arrows and numbers. In the LHSs of Figs. 4(b)-(e), outgoing modes in the drain are similarly indicated; the incoming modes remain as in Fig. 4(a). Table III also confirms that Mode 1 (2) in the source transmits to Mode 1 (2) in the drain perfectly, as required for this simple geometry, and the transmission probability total over both incident modes is identically two, as seen in the RHS of Fig. 4(a). With $V_{DS} = 0.1$ V, the CB in drain is shifted down by the applied bias, as shown in Fig. 4(b). There are still two propagating modes in the drain, but now the momentum k_x of each mode in the drain at the Fermi energy, is different from that in the source. However, drain/outgoing Mode 1 (2) remains semi-classically accessible from source/incident Modes 1 (2), and the transmission probabilities remains near unity accordingly, as again shown in Table III. (For this system, a drain mode is semi-classically reachable if and only if it can be reached via continuous variations in both k_x and E , including across the, here reduced, Brillouin zone edges, without losing more “kinetic” energy that it started with along the way—i.e., coming back to the source—and without first reaching another outgoing mode—i.e., reaching the drain). For $V_{DS} = 0.2$ V, two additional outgoing states appear in the drain, but there is little transmission probability to these new modes because they are not semi-classically reachable from the source modes. The transmission probability totaled over both incident modes remains nearly two. The situation is qualitatively similar for $V_{DS} = 0.3$ V despite an additional mode in the drain, although total injection in to Mode 1 is beginning to be degraded. For $V_{DS} = 0.4$ V and 0.5 V, however, there is only one outgoing mode in the drain (reachable semi-classically or otherwise in this case), and the totaled transmission probability drops just below one at 0 eV, as seen in Figs. 4(e) and 4(f) respectively. Therefore, the source of this NDR is the reduction of semi-classically reachable states in the drain within the range of injected carrier energies.

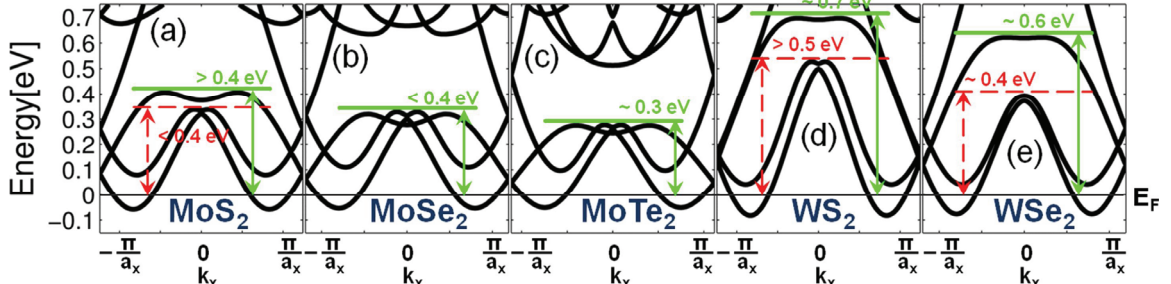


Figure 5. CB band structure of monolayer MX_2 for transverse mode $k_y = 0$, with the zero energy reference defined by an n-type doping density of $7 \times 10^{13} \text{ cm}^{-2}$. The indicated energy levels correspond to NDR behavior as exhibited in Fig.3 and described in the text.

As seen in Fig. 3(b), all simulated monolayer MX_2 n-MOSFETs exhibit NDR behaviors, but with different onset voltages V_{DS} and degree of abruptness. These differences are consistent with their band structures. Fig. 5 shows the CBs of monolayer MX_2 at a transverse mode $k_y = 0$. In each sub-figure, (a)-(e), the source-to-drain energy threshold = eV_{DS} at which the number of semi-classical source-to-drain trajectories at the source Fermi level is reduced to one, again not counting spin degeneracy, is marked with a solid (green) line. In addition, the dashed (red) line indicates when one of the semi-classical trajectories becomes at least much more convoluted, which is essentially the same energy in the case of MoSe_2 and MoTe_2 . For MoSe_2 , Fig. 5(b), the reduction to one outgoing mode occurs between $V_{\text{DS}} = 0.3$ and 0.4 V, consistent with the prior discussion. In general, the heavier the atoms, the lower the V_{DS} threshold for reduction in semi-classically available outgoing modes, with variations in the transition metal (M) atom producing the greatest change. The order in which the number of outgoing modes is reduced with V_{DS} seen in Fig. 5 is entirely consistent with the order of NDR onset in Fig. 3. Moreover, the substantial separation for the WX_2 based devices between the values of V_{DS} at which one of the semi-classical paths merely becomes much more convoluted, and when one is entirely eliminated is mirrored in the more gradual transition toward NDR. Note that the reduction in current must be completed by the V_{DS} at which the number of outgoing modes is reduced, as most evident for the MoX_2 -based devices in Fig. 3. The onset of NDR must occur earlier, particularly with the more abrupt potential variations in the self-consistent simulations of Fig. 3 than in the toy potential used for the simulations of Fig. 4. Scattering not considered here should substantially reduce if not eliminate the NDR in real devices. Still such NDR could serve as a signature of any significant quasi-ballistic transport in nano-scale TMD MOSFETs.

IV. CONCLUSION

In summary, we used atomistic full-band NEGF simulations with TB potentials obtained from DFT, to investigate the device performances of single gate monolayer MX_2 ($M = \text{Mo}, \text{W}; X = \text{S}, \text{Se}, \text{Te}$) MOSFETs. 15 nm channel length device exhibited good SS and small DIBL due to the electrostatic control afforded by the 2-D nature of monolayer MX_2 . Moreover, the large band gap characteristic of monolayer MX_2 TMDs suppress GIDL. These full band ballistic NEGF simulations also exhibit substantial NDR in the output characteristics. The source of this NDR is the reduction in outgoing states in the drain for ballistic carriers. Scattering

should moderate or eliminate the NDR in real devices, but NDR could serve as a signature of any remaining quasi-ballistic transport in nanoscale monolayer TMD n-MOSFETs.

REFERENCES

- [1] K. F. Mak, C. Lee, J. Hone, J. Shan, and T. F. Heinz, "Atomically Thin MoS_2 : A New Direct-Gap Semiconductor," *Phys. Rev. Lett.*, vol. 105, pp. 136805, 2010.
- [2] A. Splendiani, L. Sun, Y. Zhang, T. Li, J. Kim, C. Y. Chim, G. Galli, and F. Wang, "Emerging Photoluminescence in Monolayer MoS_2 ," *Nano Lett.*, vol. 10, pp. 1271–1275, 2010.
- [3] J. K. Ellis, M. J. Lucero, and G. E. Scuseria, "The indirect to direct band gap transition in multilayered MoS_2 as predicted by screened hybrid density functional theory," *Appl. Phys. Lett.*, vol. 99, pp. 261908, 2011.
- [4] S. Lebegue and O. Eriksson, "Electronic structure of two-dimensional crystals from ab initio theory," *Phys. Rev. B*, vol. 79, pp. 115409, 2009.
- [5] S. W. Han, H. Kwon, S. K. Kim, S. Ryu, W. S. Yun, D. H. Kim, J. H. Hwang, J. S. Kang, J. Baik, J. H. Shin, and S. C. Hong, "Band-gap transition induced by interlayer van der Waals interaction in MoS_2 ," *Phys. Rev. B*, vol. 84, pp. 045409, 2011.
- [6] B. Radisavljevic, A. Radenovic, J. Brivio, V. Giacometti, and A. Kis, "Single-layer MoS_2 transistors," *Nat. Nanotechnology*, vol. 6, pp. 147–150, 2011.
- [7] H. Fang, S. Chuang, T. C. Chang, K. Takei, T. Takahashi, A. Javey, "High-Performance Single Layered WSe_2 p-FETs with Chemically Doped Contacts", *Nano Lett.*, vol. 12 (7), pp. 3788–3792, 2012..
- [8] Y. Yoon, K. Ganapathi, and S. Salahuddin, "How good can monolayer MoS_2 transistors be?," *Nano Lett.*, vol. 11 (9), pp. 3768–3773, 2011.
- [9] L. Liu, B. Kumar, Y. Ouyang, and J. Guo "Performance Limits of Monolayer Transition Metal Dichalcogenide Transistors," *IEEE Trans. on Electron Devices*, vol. 58, p. 3042, 2011.
- [10] A. A. Al-Hilli and B. L. Evans, "The preparation and properties of transition metal dichalcogenide single crystals," *J. Cryst. Growth*, vol.15, pp. 93, 1972.
- [11] T. Ozaki and H. Kino, "Efficient projector expansion for the ab initio LCAO method," *Phys. Rev. B*, vol. 72, no. 045121, 2005.
- [12] J. P. Perdew, K. Burke and M. Ernzerhof, "Generalized Gradient Approximation Made Simple," *Phys. Rev. Lett.*, vol. 77, pp. 3865-3868, 1996.
- [13] A. Kumar, and P. K. Ahluwalia, "Tunable dielectric response of transition metals dichalcogenides MX_2 ($M = \text{Mo}, \text{W}; X = \text{S}, \text{Se}, \text{Te}$): Effect of quantum confinement," *Physica B*, vol. 407, pp. 4627-4634, 2012.
- [14] H. Weng, T. Ozaki, and K. Terakura, "Revisiting magnetic coupling in transition-metal-benzene complexes with maximally localized Wannier functions," *Phys. Rev. B*, vol. 79, no. 235118, 2009.
- [15] T. Usuki, M. Saito, M. Takatsu, R. A. Kiehl, and N. Yokoyama, "Numerical analysis of ballistic-electron transport in magnetic fields by using a quantum point contact and a quantum wire," *Phys. Rev. B*, vol. 52, pp. 8244-8255, 1995.
- [16] J. Chang, L. F. Register, and S. K. Banerjee, " Atomistic Full-Band Simulations of Monolayer MoS_2 Transistors," arXiv:1304.2990.